


# Simulating cosmological evolution by quantum quench of an atomic Bose-Einstein condensate

Ke Wang<sup>1,2</sup>, Han Fu<sup>3</sup>, and K. Levin<sup>1</sup>

<sup>1</sup>*Department of Physics and James Franck Institute, University of Chicago, Chicago, Illinois 60637, USA*

<sup>2</sup>*Kadanoff Center for Theoretical Physics, University of Chicago, Chicago, Illinois 60637, USA*

<sup>3</sup>*Department of Physics, College of William and Mary, Williamsburg, Virginia 23187, USA*

 (Received 20 April 2023; revised 7 August 2023; accepted 15 December 2023; published 18 January 2024)

In cosmological evolution, it is the homogeneous scalar field (inflaton) that drives the universe to expand isotropically and to generate standard model particles. However, to simulate cosmology, atomic gas research has focused on the dynamics of Bose-Einstein condensates (BEC) with continuously applied forces. In this paper we argue that a complementary approach needs also to be pursued; we thus consider the analog BEC experiments in a nondriven and naturally closed atomic system. We implement this using a BEC in an optical lattice which, after a quench, freely transitions from an unstable to a stable state. This dynamical evolution displays the counterpart “preheating,” “reheating,” and “thermalization” phases of cosmology. Importantly, our studies of these analog processes yield tractable analytic models. Additionally, of great utility to the cold atom community, such understanding elucidates the dynamics of nonadiabatic condensate preparation. Indeed, the dynamical processes discussed here are generic and in future cold atom reequilibration experiments it will be important to observe both the preheating stage, corresponding to a fragmented condensate, and the reheating stage, corresponding to a particle cloud.

DOI: [10.1103/PhysRevA.109.013316](https://doi.org/10.1103/PhysRevA.109.013316)

## I. INTRODUCTION

Recent excitement in the literature has drawn attention to quantum field simulators of cosmological evolution as implemented in cold atom systems [1–14]. Such studies are motivated by the fact that atomic physics laboratories provide the possibility of studying in real time and in a reproducible fashion, the analog of extreme nonequilibrium [15–21] conditions such as might have prevailed in the early universe. Much of the emphasis, both in experiment [1,3,12] and theory [22–24] has focused on the inflation stage. Equally important are the three subsequent stages which have received some attention [3,11] as well.

A paradigmatic cosmological example which describes the evolution of the early universe is the “slow roll inflation” scenario [25–30]. The crucial features of this scenario are that (1) the universe is an isolated quantum system in which inflationary processes proceed on their own. (2) This scenario begins with a homogeneous scalar inflaton field  $\varphi$  having high energy; the subsequent dynamics correspond to  $\varphi$  slowly rolling down a potential energy hill towards equilibration. After an exponentially slow inflation period at the beginning, (3) the inflaton oscillates and transfers its energy to matter fields involving an explosive particle production, and then finally to thermalization. This cosmological model, importantly, has a body of experimental support [25,26]. These processes are illustrated schematically in the simple picture of Fig. 1(a).

In this paper we capture these three essential features of cosmology (after inflation) by studying the dynamics of a dilute Bose gas on an optical lattice, transitioning from an unstable to a stable Bose-Einstein condensate (BEC). Our unstable BEC is formed in an optical lattice configuration through a quench that instantaneously pumps particles from a

lower to an upper band. Unlike the other atomic physics platforms [3,11,12] ours is an isolated system which starts from a homogeneous BEC. The evolutionary dynamics proceeds on its own without external drive so that all the dynamics we observe after the quench is driven by the excited BEC or “inflaton.”

We find that this high-energy BEC state which is intrinsically unstable, spontaneously transfers its energy to inhomogeneous quantum fluctuations and finally transitions to a stable (condensate) state. The dynamical path is described by three evolutionary stages with striking similarity to the three postinflation stages of inflaton dynamics. Its subsequent evolution corresponds qualitatively to the simple dynamics suggested in Fig. 1(b).

By exploiting this correspondence, our paper demonstrates how cold atom systems can provide *concrete*, analytically tractable models for the dynamics within each of these evolutionary stages of the early universe. Accompanying our analytics are demonstrably consistent Gross-Pitaevskii simulations which establish the relative time intervals associated with each of the three stages. Moreover, the thermalized state or endpoint contemplated here is a recondensation in contrast to previously studied cosmological analog systems. Thus, this work should satisfy a centrally important objective of cold atom research: to create and to more deeply understand the pathways associated with the nonadiabatic preparation of exotic condensate phases [31–33].

Figure 2(a) provides an illustration of the proposed experiment. The momentum distributions of the immediate postquench stage and that of the three subsequent evolutionary stages obtained from our simulations are represented by the snapshots in Fig. 2(b). The first of the later three (corresponding to “preheating” in the cosmological literature)

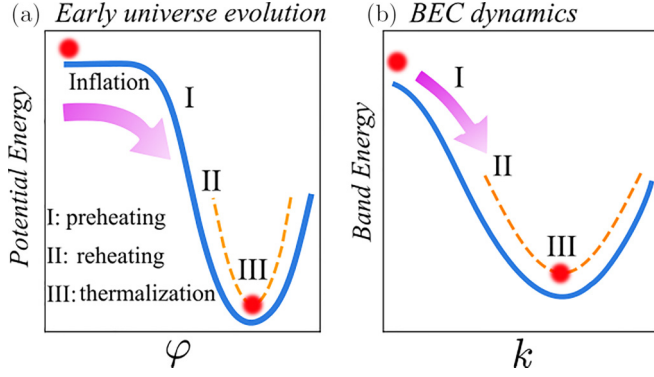


FIG. 1. Similarity of systems which transition from an unstable to a thermal state. (a). Slow roll inflation picture reflecting how the inflaton slowly rolls down the potential and ultimately generates the standard model particles. (b). A Bose-Einstein condensate initially at an unstable state similarly rolls down to relax into the true ground state, corresponding to the band minimum.

yields, through a parametric resonance, what we refer to as a “ring condensate” [34]. More precisely, this so-called “condensate” corresponds to a macroscopic occupation of many finite momentum modes (as in a fragmented condensate), but distributed in a ring geometry, as seen in the second panel of Fig. 2(b).

Collisions between the initial and ring condensates lead to a second stage (“reheating”) which ends with a destruction of both condensates and a proliferation of nonthermal bosonic quasiparticles having a range of different momenta, which is seen in the third panel of Fig. 2(b) and which we refer to as a *cloud state*. The formation of this cloud, in which all phase coherence is lost is, in turn, a crucial step that then

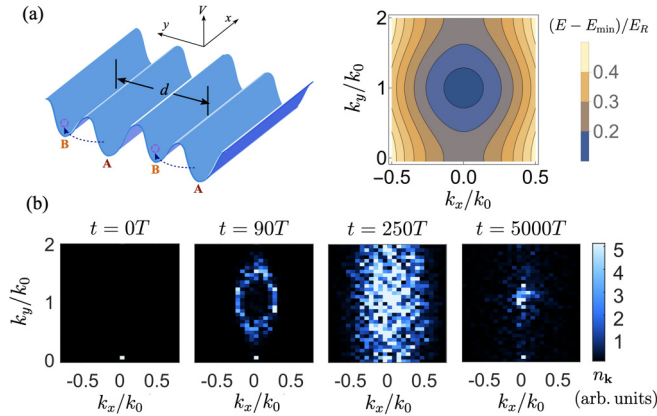


FIG. 2. Optical lattice setup and numerical results. (a). Left panel: Schematic plot of the two-dimensional optical lattice potential confining atoms. The unit cell consists of two sites  $A$  and  $B$ . Pink circles in (a) denote atoms. Right panel: Color contour of the upper band structure. Here momentum is given in units of  $k_0 = \pi/d$ . Here  $k = 0$  is a saddle point in two dimensions and a local maximum along the  $k_y$  direction. (b). Momentum-space atom distribution  $n_{\mathbf{k}} = |\psi(\mathbf{k})|^2$  at different stages from GP simulations at given interaction strength. Here  $\psi(\mathbf{k})$  is the Fourier transform of  $\psi(\mathbf{r})$ . Here the units of time are in recoil energy  $E_R$ ; for convenience in plotting we take  $T$  to be  $h/(4E_R)$ . For numerical details see Appendix E.

enables the system to reach the third stage corresponding to full thermalization shown in the fourth panel Fig. 2(b).

## II. NUMERICAL SIMULATION

As is illustrated in Fig. 2(a), we start with a two-dimensional system where the Bose atoms are confined in the  $y$  direction by a periodic potential  $V(y) = V_1 \sin(4\pi y/d) + V_2 \sin(2\pi y/d)$  with a free particle dispersion in the  $x$  direction. Here  $V(y)$  involves two sublattices (denoted as  $A/B$  sites) with a potential offset controlled by  $V_2$ . The potentials of  $A$  and  $B$  are exchanged during the quench, which effectively pumps atoms from  $A$  sites to  $B$  sites, thereby exciting the BEC from the lower band to the upper band. The extra free dimension in Fig. 2(a) plays an essential role [33,35] in the recondensation process, as it provides high-energy states needed to absorb the released kinetic energy when the BEC reforms in the end. The results here can be readily extended to three-dimensional (3D) systems with only quantitative changes.

In our simulations, we use a CUDA-based Gross-Pitaevskii equation solver implemented on graphic processing units, based on a split-step algorithm [36,37] with no dissipation added:  $i\hbar \frac{\partial}{\partial t} \Psi(\mathbf{r}, t) = (-\frac{\hbar^2 \nabla^2}{2m} + V(y) + g|\Psi(\mathbf{r}, t)|^2) \Psi(\mathbf{r}, t)$ , where  $m$  is the boson mass, and  $g$  the interaction strength. Details of the simulations and parameters are discussed in Appendix E.

To make contact with cosmology we note that in the cold atom laboratory, a quantum quench of the BEC to the upper band is the analog creation of a homogeneous oscillating inflaton field. The quenched BEC is associated with a finite oscillation frequency  $\omega \sim J/\hbar$ , where  $J$  corresponds to the width of the upper band with dispersion  $\epsilon_{\mathbf{k}} = \hbar^2 k_x^2/2m + |J| \cos(k_y d)$ . The subsequent dynamics is essentially confined to the upper band since the interaction-mediated tunneling between two bands is tuned to be negligibly small. We presume  $gn_0/J < 1$  (where  $n_0$  is the condensate density) and from our tight-binding limit simulations determine the value for  $J \approx 0.05E_R$  in recoil units. It is this finite-frequency BEC which serves as an internal driving source to pump particles out of the condensate, leading to its fragmentation and eventual disappearance.

## III. PREHEATING: EARLY DYNAMICS

In cosmological models, at the end of the inflation period the inflaton field is assumed to oscillate around the minimum of its potential and in this way decay into other forms of matter. This next stage following inflation is called preheating [38–40], where the universe is populated via parametric resonances. The coherent nature of the BEC inflaton enhances the efficiency of particle production and at early times particles (inhomogeneous fluctuations) are generated exponentially.

Analogously, these parametric resonances emerge in the cold atom system during the preheating stage which is associated with an effective preheating Hamiltonian [41]

$$\hat{H}_{\text{eff}}^p = \sum_{\mathbf{k} \neq 0} \epsilon'(\mathbf{k}) \hat{a}_{\mathbf{k}}^\dagger \hat{a}_{\mathbf{k}} + \frac{gn_0}{2} \sum_{\mathbf{k} \neq 0} (\hat{a}_{\mathbf{k}}^\dagger \hat{a}_{-\mathbf{k}}^\dagger + \hat{a}_{\mathbf{k}} \hat{a}_{-\mathbf{k}}). \quad (1)$$

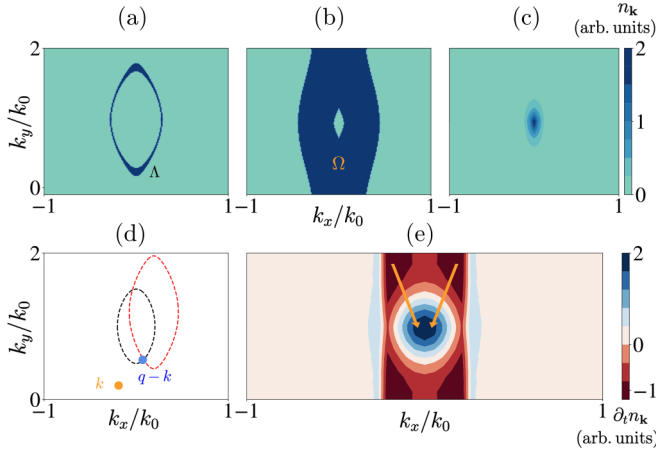


FIG. 3. Evolutionary stages derived from analytic theory [(a)–(c)], which should be compared with simulations in Fig. 2(b). Here, the ring stage (a) originates from a parametric instability while (b) the cloud stage arises from collisions between two condensates. The quasithermal distribution (c) derives from Boltzmann dynamics. (d) Characterization of the  $\mathbf{k}$  and  $\mathbf{q}-\mathbf{k}$  pairs which lead to cloud formation and derive from momentum and energy conservation [42] (e) Distribution of the rate of change of particle number  $\partial_t n_{\mathbf{k}}$ . The plot presents this distribution at early times where Boltzmann dynamics is applicable. The arrows show how particles flow to the band minima.

Here  $\epsilon'(\mathbf{k}) = \epsilon_{\mathbf{k}} - J + gn_0$ ,  $\hat{a}_{\mathbf{k}}$  is a bosonic operator. The presence of imaginary eigenvalues  $\lambda(\mathbf{k}) \equiv \sqrt{\epsilon'(\mathbf{k})^2 - g^2 n_0^2}$  of Eq. (1) (when  $|\epsilon'(\mathbf{k})| < gn_0$ ) reflects exponential growth of the new condensate particles. The resonance condition  $\epsilon_{\mathbf{k}} = J - gn_0$  corresponds, in momentum space to a ring-shaped additional fragmented condensate, which forms on a timescale  $t_r \sim \hbar(gn_0)^{-1} \ln L$ . Here  $L$  denotes the system size. These predictions are confirmed by the GP simulations shown in the second panel of Fig. 2(b). The dynamics can be described by an analog of the Mathieu equation, for details see Appendix D.

#### IV. REHEATING STAGE

The universe enters the reheating stage once the energy of the newly populated degrees of freedom becomes nonnegligible. Here the inflaton continues to oscillate and interact with its fragmented products (called rescattering); this is associated with nonlinear dynamics. At the same time the energy of the inflaton and its byproducts is transferred to standard model particles. The accompanying phenomenology of this process in cosmological models is complex. There may emerge turbulent scaling [43], or oscillons [44,45] or solitons [46] and cosmic defects.

In the cold atom setup, the formation of the ring-condensate in momentum space shown in Fig. 3(a) marks the start of the reheating stage. In this stage, the quenched BEC (inflaton) continues to oscillate at high frequency and interactions between the BEC and the ring products become important. Particles are pumped out of these byproducts and energy is transferred to other noncondensed particles. These dynamical processes eventually generate a highly nonequilibrium “cloud” phase shown in the third panel of Figs. 2(b) and 3(b).

It is convenient at this point to introduce a characterization of the momentum regime occupied by the ring condensate; we call this  $\Lambda$  throughout the paper [see Fig. 3(a)]. One important interaction effect,  $V_{\Lambda, \Lambda}$ , corresponds to the annihilation of two particles in the ring condensate. These collision events, the details of which are discussed in Appendix B, are associated with back-reaction dynamics and broaden the radius of the ring. More important is the second process  $V_{0, \Lambda}$  which annihilates particles from both condensates and leads to the destruction of condensates associated with an effective reheating Hamiltonian

$$\hat{H}_{\text{eff}}^{\mathbf{0}, \mathbf{r}} \equiv \sum_{\mathbf{q} \notin \Lambda} \epsilon''_{\mathbf{q}} \hat{a}_{\mathbf{q}}^\dagger \hat{a}_{\mathbf{q}} + U' \sum_{\mathbf{k} \in \Lambda, \mathbf{q} \notin \Lambda} (\hat{a}_{\mathbf{q}}^\dagger \hat{a}_{\mathbf{k}-\mathbf{q}}^\dagger + \text{H.c.}) + U' \sum_{\mathbf{k} \in \Lambda, \mathbf{q} \notin \Lambda} (\hat{a}_{\mathbf{q}}^\dagger \hat{a}_{\mathbf{q}-\mathbf{k}} + \text{H.c.}) \quad (2)$$

Here  $\epsilon''_{\mathbf{q}} = \epsilon_{\mathbf{q}} - (J - gn_0/2 + g\bar{n}_r/2 - g\bar{n}_0/2)$  is an effective kinetic energy and  $U' = 2g\sqrt{\bar{n}_0\bar{n}_r}/L_r$  is the effective interaction strength for these back-reaction processes with  $L_r$  being the number of modes in the ring. Additionally,  $\bar{n}_{0,r}$  is the respective density for each coexisting condensate. The derivation of Eq. (2) is given in Appendix B.

In contrast to Eq. (1), where the physics is local in  $\mathbf{k}$  space, the Hamiltonian in Eq. (2) is intrinsically nonlocal. These nonlocal features, reflecting the extended ring condensate, are generic and universal and pertain to a geometrically extended “resonance band” in  $\mathbf{k}$  space. The physical consequences of Eq. (2) are that the eigenvalue spectrum now involves a large number of *complex* values,  $\lambda_i$  where the range of  $i$  scales with the system size. These complex eigenvalues suggest an interpretation in which there is a proliferation of bosonic particles concurrent with the decay of the condensate(s).

To understand the origin of these complex eigenvalues and the time evolution more quantitatively, we note that the dynamics associated with Eq. (2) can be derived using a  $2 \times 2$  matrix; since the effective interaction  $U'$  is small, each pair  $(\mathbf{k}, \mathbf{q} - \mathbf{k})$  can be treated separately. This corresponds to an equation of motion

$$\frac{d}{dt} \begin{pmatrix} \hat{a}_{\mathbf{k}}(t) \\ \hat{a}_{\mathbf{q}-\mathbf{k}}^\dagger(t) \end{pmatrix} \simeq \frac{-i}{\hbar} \begin{pmatrix} \epsilon''_{\mathbf{k}} & U' \\ -U' & -\epsilon''_{\mathbf{q}-\mathbf{k}} \end{pmatrix} \begin{pmatrix} \hat{a}_{\mathbf{k}}(t) \\ \hat{a}_{\mathbf{q}-\mathbf{k}}^\dagger(t) \end{pmatrix}, \quad (3)$$

where  $\hat{a}_{\mathbf{k}}(t)$  evolves under the effective Hamiltonian in Eq. (2). The eigenvalues are given by

$$\lambda_{\pm}(\mathbf{k}, \mathbf{q} - \mathbf{k}) = \frac{\epsilon''_{\mathbf{k}} - \epsilon''_{\mathbf{q}-\mathbf{k}}}{2} \pm \sqrt{\left(\frac{\epsilon''_{\mathbf{k}} + \epsilon''_{\mathbf{q}-\mathbf{k}}}{2}\right)^2 - U'^2}, \quad (4)$$

and when  $\epsilon''_{\mathbf{k}} + \epsilon''_{\mathbf{q}-\mathbf{k}} = 0$ , one clearly sees that the corresponding values for  $\lambda$  become *complex*.

The momentum distribution ( $\Omega$ ) associated with this reheating stage is plotted in Fig. 3(b) which takes on a cloud-like form representing a proliferation of noncondensed, nonthermal bosons. Here the system enters into a highly nonequilibrium phase, where the initial condensate, ring-condensate, and a cloud-shaped distribution of nonthermal bosons coexist. This cloud, deriving from the complex eigenvalues in Eq. (2), reflects collisions between specific bosonic pairs as shown in Fig. 3(d). Here the energy and momentum

conservation constraints, indicated by the two dashed lines, establish how to associate the value of  $q - k$  with a given  $k$  in the pair. The reheating stage ends finally with the complete decay of the condensate and the full formation of the cloud state.

This condensate decay is the cold gas counterpart of the cosmological analog in which at the end of reheating one has the generation of standard model particles. Here one sees a destruction of all vestiges of phase coherence observed in the earlier evolutionary stages, in many ways similar to the cosmological picture in which the original memory of the (inflaton-)condensate completely disappears.

## V. LATE TIME: THERMALIZATION

In cosmology, the reheating stage ends with the complete decay of the inflaton field and a highly nonthermal distribution of standard model particles. All important particles which will ultimately evolve to thermal equilibrium are already generated. What follows next is a stage of thermalization in which energy is redistributed among the particles; this enables them to reach an equilibrium distribution, as supported by cosmological evidence [47].

In a similar way to the cold atom system, the quenched condensate completely disappears and a highly nonthermal distribution of particles emerges, marking the end of the reheating stage. Thermalization then follows; here all finite-momentum degrees of freedom equilibrate as the system relaxes towards thermal equilibrium. We find that the dynamics in this stage is well described by a quantum Boltzmann equation. This evolves the nonthermal cloud state to a quantum Bose-Einstein distribution with, as it turns out, nearly 20% of particles in the condensate.

In this Boltzmann-like description of the dynamics the interaction energy is assumed to be much smaller than the bandwidth so that it can be treated perturbatively. This leads to the famous quantum kinetic Boltzmann equation for a Bose gas [48],

$$\partial_t n_{\mathbf{k}} = I(\{n_{\mathbf{k}'}\}). \quad (5)$$

Here  $n_{\mathbf{k}}$  is the particle number distribution function and  $I(\{n_{\mathbf{k}'}\})$  is the collision integral. Perturbatively, we have that  $I(\{n_{\mathbf{k}'}\})$  depends on

$$\begin{aligned} \Gamma(\mathbf{k}, \mathbf{k}'; \mathbf{k} + \mathbf{q}, \mathbf{k}' - \mathbf{q}) &= n_{\mathbf{k}-\mathbf{q}} n_{\mathbf{k}'+\mathbf{q}} (1 + n_{\mathbf{k}}) (1 + n_{\mathbf{k}'}) \\ &\quad - (n_{\mathbf{k}-\mathbf{q}} + 1) (n_{\mathbf{k}'+\mathbf{q}} + 1) n_{\mathbf{k}} n_{\mathbf{k}'}. \end{aligned} \quad (6)$$

Here  $\mathbf{k}'$  and  $\mathbf{q}$  are integrated out to yield the collision term  $I = 2\hbar^{-1} g^2 \int d^2 \mathbf{k}' d^2 \mathbf{q} (2\pi)^{-3} \Gamma \delta(E_i - E_f)$ , where, for simplicity of notation, we dropped the arguments in  $\Gamma$ ; the  $\delta(E_i - E_f)$  term introduces conservation of kinetic energy. This collision integral then determines the momentum and energy flow processes which lead the system to equilibration.

Because of the special property of the cloud state, initially, the main contribution to  $\Gamma$  is from scattering events involving one out-of-cloud and three in-cloud modes. The details of the scattering events are described in Appendix C. In such events,  $\Gamma$  is dominated by the cubic terms [48]  $\sim n^3$ . More specifically, the important collisions derive from two intermediate-energy particles in the cloud which scatter into one low-energy mode

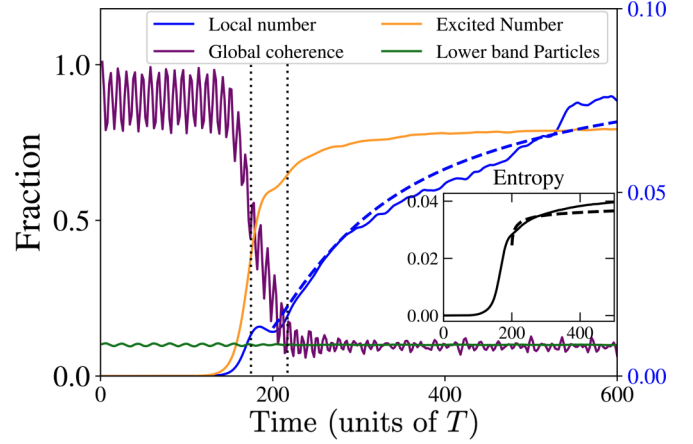


FIG. 4. Time evolution of key properties from GP simulations. Beyond  $600T$  the behavior is rather stable. The y axis for blue lines is on the right, while the left axis pertains to all other curves. The solid and dashed blue lines compare the particle number  $n_{\mathbf{k}}$  near the band minima from GP and analytical Boltzmann calculations, respectively. The purple curve reflects global phase coherence while the orange line plots the total particle number in excited states excluding the  $\mathbf{k} = 0$  mode. The green curve indicates the residual particle number in the lower band, and is responsible for the oscillatory behavior found in the global coherence plots. Vertical black dotted lines indicate the time interval over which there is a smooth crossover between different evolutionary stages. The inset compares the entropy per particle from GP simulations (solid) and Boltzmann theory (dashed) using  $S = N^{-1} \sum_{\mathbf{k}} [(1 + n_{\mathbf{k}}) \ln(1 + n_{\mathbf{k}}) - n_{\mathbf{k}} \ln(n_{\mathbf{k}})]$ , where  $N$  is the total particle number. This monotonically increasing entropy and its final saturation at long times are consistent with equilibration.

around the band minimum and the other mode at high energy. The flow of particles is shown in Fig. 3(e). As a result, Eq. (5) is of the form  $\partial_t n_{\mathbf{k}} \propto g^2 n_0^3$ . As a consequence of the relatively time-independent particle distribution, it follows that the initial dynamics evolving from the cloud yields a linear-in-time growth for the occupation of the band minimum.

As the dynamics continues to evolve in time the system will eventually be driven towards a Bose-Einstein distribution. In this regime, the quadratic term  $n_{\mathbf{k}-\mathbf{q}} n_{\mathbf{k}'+\mathbf{q}} - n_{\mathbf{k}} n_{\mathbf{k}'}$  in  $\Gamma$  begins to dominate and the time variation of the particle distribution slows down, approaching the quantum distribution function  $n_{\mathbf{k}}^{\text{eq}} = (e^{\beta(\epsilon_{\mathbf{k}} - \mu)} - 1)^{-1}$ , as expected. Here the inverse temperature  $\beta$  in this equilibrium state is determined by the kinetic energy of the initial cloud while the chemical potential  $\mu$  approaches zero for sufficiently large system sizes. In this way we establish *condensation* at the band minima in the thermodynamical limit.

## VI. COMPARISON BETWEEN ANALYTICS AND SIMULATIONS

We turn now to Fig. 4, which summarizes the evolutionary stages as found in the GP simulations and presents comparisons with our analytics, demonstrating reasonable consistency. There are multiple time-dependent functions indicated by the curves. At early times (of the order of  $t_1 \propto g^{-1}$ ) the simulations show that there is a rapid growth in occupation of excited modes (orange curve) which reflects the

formation of a new ring-like condensate. The governing dynamics shows an exponential growth rate, as expected in a parametric resonance. Following this, in the second stage, the system experiences a complete loss of global phase coherence (purple curve) associated with the upper band, which corresponds to the cloud stage. Following this stage, then, the occupation number in the band minimum (solid blue curve) grows appreciably, displaying the expected linear time dependence for an extended range of intermediate times.

The number of particles at the band minimum is shown in Fig. 4 via a comparison between simulations (solid) and Boltzmann analytical calculations (dashed) blue curves, indicating that both overlap reasonably well. This stage of thermalization is reflected in the growth of the (H theorem) entropy as well, which is plotted as analogous dashed and solid lines in the inset to Fig. 4.

## VII. CONCLUSION

This paper has shown how the intrinsic dynamics of a Bose condensate in an optical lattice transitioning from an unstable to a stable BEC provides an analog experiment for the slow roll inflation cosmology scenario. Importantly, it represents a homogeneous and a closed quantum system in which the inflationary processes proceed without the external drive which is usually incorporated in these analog laboratories [1–14]. All of these are exciting contributions which address cosmology as seen through the lens of a quantum gas.

The present equilibration study also informs about cold atom engineering of exotic condensate phases which should be of direct interest to the cold atom community. Importantly, we argue here that the dynamical processes are quite generic and in future recondensation experiments it will be important to observe both the preheating stage, corresponding to a fragmented condensate and the reheating stage, corresponding to a particle “cloud.”

As an example, the upper-band condensation discussed here should be relatively straightforward to implement experimentally, as was suggested in a previous theoretical study [31], although there, while the cloud stage was found, the antecedent preheating stage and associated ring condensate were not. Retrospectively, we note that, in previous simulations [33] involving a dynamical preparation of an atomic condensate in a Hofstadter band, there were, indeed, indications of condensate fragmentation [49]. We caution, however, that once the interactions become sufficiently strong the production of particles is much more efficient so that the formation of the cloud state is almost immediate. Interestingly, such behavior is well known in the cosmology literature [50] and associated with the “broad resonance” regime.

Equally important, we stress that the present studies provide analytically tractable models for the dynamics within each of these evolutionary stages. This should be of value both for simple cosmological models and for future analyses of dynamical engineering in cold atom systems.

## ACKNOWLEDGMENTS

We thank Cheng Chin for his substantial help in writing this manuscript. Additionally, we are very grateful to Erich

Mueller for calling attention to the specific quench protocol studied here. This work was partially (KL, KW) supported by the Department of Energy (Grant No. DE-SC0019216). HF acknowledges support from DOE, Grant No DE-SC002245. We thank Andreas Glatz for valuable help and insight over many years of collaborations. We also acknowledge Steven Wu, D. T. Son, L. T. Wang, S. Koren, A. Lucas, Y. M. Zhong, and G. H Zhou for helpful discussions.

## APPENDIX A: DYNAMICS IN THE PREHEATING STAGE

To begin, we address the early dynamics in the preheating stage, focusing on an effective theory of the upper band degrees of freedom, with the effective Hamiltonian

$$H_{\text{upper}} = \sum_{\mathbf{k}} \epsilon_{\mathbf{k}} \hat{a}_{\mathbf{k}}^{\dagger} \hat{a}_{\mathbf{k}} + \frac{g}{2V} \sum_{\mathbf{k}, \mathbf{k}', \mathbf{q}} \hat{a}_{\mathbf{k}}^{\dagger} \hat{a}_{\mathbf{k}'}^{\dagger} \hat{a}_{\mathbf{k}'-\mathbf{q}} \hat{a}_{\mathbf{k}+\mathbf{q}}. \quad (\text{A1})$$

Here  $\epsilon_{\mathbf{k}} = \hbar^2 k_x^2 / 2m + |J| \cos(k_y d)$  is the upper-band dispersion and  $\hat{a}_{\mathbf{k}}, \hat{a}_{\mathbf{k}}^{\dagger}$  are bosonic operators in this band,  $J$  is the hopping parameter associated with the periodic potential treated here in a tight-binding approximation. To obtain  $J$ , we directly diagonalize the original Hamiltonian matrix based on the implemented lattice potential with a size cutoff where a convergence is achieved.  $J$  is exponentially dependent on the lattice depth (dominated by  $V_1$  here) while the band gap between the first and second bands are tuned by  $V_2$ . Because of the macroscopic occupation of a pumped BEC, we focus on the dynamics of scattering events associated with  $\mathbf{k} = \mathbf{0}$  modes. This leads to a many-body interaction term

$$\hat{V}_0 \equiv \frac{g}{2V} \left( \hat{a}_0^{\dagger} \hat{a}_0^{\dagger} \hat{a}_0 \hat{a}_0 + \sum_{\mathbf{k}} (\hat{a}_{\mathbf{k}}^{\dagger} \hat{a}_{-\mathbf{k}}^{\dagger} \hat{a}_0 \hat{a}_0 + \text{H.c.}) + 4 \sum_{\mathbf{k}} \hat{a}_{\mathbf{k}}^{\dagger} \hat{a}_0^{\dagger} \hat{a}_{\mathbf{k}} \hat{a}_0 \right). \quad (\text{A2})$$

It is useful to rewrite this expression using  $\hat{a}_0^{\dagger} \hat{a}_0 = N - \sum_{\mathbf{k} \neq 0} \hat{a}_{\mathbf{k}}^{\dagger} \hat{a}_{\mathbf{k}}$  where the scalar  $N$  is the total number of particles in the system. Using this replacement, one finds a quadratic effective Hamiltonian describing the scattering events between condensed and noncondensed particles [41]

$$\hat{H}_{\text{eff}}^p = \sum_{\mathbf{k} \neq 0} \epsilon'_{\mathbf{k}} \hat{a}_{\mathbf{k}}^{\dagger} \hat{a}_{\mathbf{k}} + \frac{gn_0}{2} \sum_{\mathbf{k} \neq \mathbf{k}} (\hat{a}_{\mathbf{k}}^{\dagger} \hat{a}_{-\mathbf{k}}^{\dagger} + \hat{a}_{\mathbf{k}} \hat{a}_{-\mathbf{k}}). \quad (\text{A3})$$

Here  $\epsilon'_{\mathbf{k}} = \epsilon_{\mathbf{k}} - J + gn_0$ ,  $n_0 = N/V$ , and we ignored all quantum fluctuations from noncondensed particles. This yields Eq. (3) in the main text. In the Heisenberg picture, we address the time evolution of operators under this effective Hamiltonian

$$\hat{a}_{\mathbf{k}}(t) = e^{i\hat{H}_{\text{eff}}^p t / \hbar} \hat{a}_{\mathbf{k}} e^{-i\hat{H}_{\text{eff}}^p t / \hbar}. \quad (\text{A4})$$

From the commutation relations it is seen that

$$\frac{d}{dt} \begin{bmatrix} \hat{a}_{\mathbf{k}}(t) \\ \hat{a}_{-\mathbf{k}}^{\dagger}(t) \end{bmatrix} = \frac{-i}{\hbar} \begin{bmatrix} \epsilon'_{\mathbf{k}} & gn_0 \\ -gn_0 & -\epsilon'_{\mathbf{k}} \end{bmatrix} \begin{bmatrix} \hat{a}_{\mathbf{k}}(t) \\ \hat{a}_{-\mathbf{k}}^{\dagger}(t) \end{bmatrix}. \quad (\text{A5})$$

Note that the  $2 \times 2$  matrix here is non-Hermitian so that the dynamics are nonunitary.

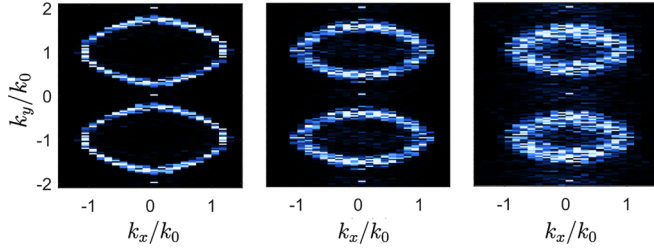


FIG. 5. Ring formation during the preheating stage, as represented by a momentum-space distribution. From left to right the interaction energy is increased as  $gn_0 = 0.0075E_R$ ,  $0.0151E_R$ ,  $0.0226E_R$ .  $n_{\mathbf{k}} = |\psi(\mathbf{k})|^2$ . A clear scaling of ring width with the interaction energy determined by the resonance condition is seen.

From the matrix eigenvalues

$$\omega_{\mathbf{k}} = \sqrt{\epsilon_{\mathbf{k}}'^2 - g^2 n_0^2 / \hbar}, \quad (\text{A6})$$

it follows that  $\omega_{\mathbf{k}}$  becomes imaginary when  $\epsilon_{\mathbf{k}}'^2 - g^2 n_0^2 < 0$  which is to be associated with exponential growth in the number of particles. The condition  $\epsilon_{\mathbf{k}}' = gn_0$  provides the boundary separating the dynamics associated with that of conventional Bogoliubov quasiparticles and that associated with a parametric instability leading to the growth of a ring condensate, as discussed in the main text.

The ring center is determined by

$$\hbar^2 k_x^2 / 2m + J \cos(k_y d) = J - gn_0. \quad (\text{A7})$$

Since  $\cos(k_y d)$  is periodic in momentum space, this leads to a closed ring.

Moreover, the boundary region for exponential growth corresponds to the onset of imaginary eigenvalues; this is associated with the condition  $|\epsilon_{\mathbf{k}}'| = gn_0$ . At this boundary the modes are static, having zero frequency.

### Connection to GP simulation results

From Eq. (A7), one sees that the ring position is directly determined by the interaction strength. This is confirmed by numerical simulations, see Fig. 5. A more quantitative analysis is summarized in Table I, where a scaling of the ring position and growth exponent is shown.

## APPENDIX B: DYNAMICS IN THE REHEATING STAGE

The appearance of a second condensate (through ring formation) is an important step en route to thermalized recondensation. Crucial here is that now two condensates are present which can lead to intercondensate scattering events. The ring is not a replacement of the original condensate but rather represents a fragmentation.

### 1. Back-reaction: Balancing between $k = 0$ and ring condensate

In this subsection which is associated in the cosmological context with “back-reaction,” we study the scattering events within ring condensates, first establishing a mechanism to enable a coexisting BEC (corresponding to simultaneous

TABLE I. Summary of characteristic timescale and position for the ring formation at different interaction strengths.  $E_R/h = 1.3$  kHz,  $2\pi/T = 6300$  Hz,  $\omega_0 = 1$  Hz. Here  $k_y$  is identified as the smallest  $y$ -momentum value in the ring, which corresponds to the  $k_x = 0$  point in the equienergy ring in Fig. 5. The time is chosen such that the particle density at this  $k_y$  has grown to around 1000 (arb.units). Here the energy difference  $\Delta E = E(0, k_y) - E_0$  is measured with respect to the initial energy  $E_0 = -2.07237E_R$  at  $\mathbf{k} = 0$  in the second band. One can see a scaling of  $1/t$  and  $\Delta E$  as  $\propto gn_0$ . Considering the error of  $\Delta t \sim 10T$ ,  $\Delta k_y \sim 0.03k_0$  in the numerical data, the scaling relation is reasonably well satisfied.

$gn_0/(h\omega_0)$	$t/T$	$k_y/k_0$	$\Delta E/E_R$
10	310	0.28	-0.0189
20	160	0.44	-0.0425
30	110	0.56	-0.0620
40	90	0.75	-0.0892

ring and  $k = 0$  condensates). Ultimately, in the “rescattering” phase, collisions between the two lead to a destabilization.

Once a ring BEC has formed, one has to consider scattering events involved with ring modes. Here there are four terms to consider:

$$\begin{aligned} \hat{V}_{r,r} \equiv \frac{g}{2V} & \left( \sum_{\mathbf{q}_1, \mathbf{q}_2 \in \Lambda} \sum_{\mathbf{q}_3, \mathbf{q}_4 \in \Lambda} + \sum_{\mathbf{q}_1, \mathbf{q}_2 \in \Lambda} \sum_{\mathbf{q}_3, \mathbf{q}_4 \notin \Lambda} \right. \\ & \left. + \sum_{\mathbf{q}_1, \mathbf{q}_2 \notin \Lambda} \sum_{\mathbf{q}_3, \mathbf{q}_4 \in \Lambda} + 4 \sum_{\mathbf{q}_1, \mathbf{q}_3 \in \Lambda} \sum_{\mathbf{q}_2, \mathbf{q}_4 \notin \Lambda} \right) \\ & \times \hat{a}_{\mathbf{q}_4}^\dagger \hat{a}_{\mathbf{q}_3}^\dagger \hat{a}_{\mathbf{q}_2} \hat{a}_{\mathbf{q}_1} \delta(\mathbf{q}_1 + \mathbf{q}_2 - \mathbf{q}_3 - \mathbf{q}_4). \quad (\text{B1}) \end{aligned}$$

Since the ring is an extended object, the first summation itself contains two types of contributions: (1) forward scattering events (such as  $\sum_{\mathbf{q}_1, \mathbf{q}_2 \in \Lambda} 2\hat{a}_{\mathbf{q}_1}^\dagger \hat{a}_{\mathbf{q}_2}^\dagger \hat{a}_{\mathbf{q}_2} \hat{a}_{\mathbf{q}_1}$ ); (2) the scattering involving two incident particles with opposite momenta ( $\sum_{\mathbf{q}_1, \mathbf{q}_2 \in \Lambda} \hat{a}_{\mathbf{q}_1}^\dagger \hat{a}_{-\mathbf{q}_1}^\dagger \hat{a}_{\mathbf{q}_2} \hat{a}_{-\mathbf{q}_2}$ ). In the second or third summation, the case  $\mathbf{q}_1 = -\mathbf{q}_2$  is the leading contribution while all other are subleading [51]. In the fourth summation, the leading contribution corresponds to  $\mathbf{q}_1 = \mathbf{q}_3$ .

It follows that  $\hat{V}_{r,r}$  can be approximated by

$$\begin{aligned} \hat{V}_{r,r} \simeq \frac{g}{2V} & \left( \sum_{\mathbf{q}_1, \mathbf{q}_2 \in \Lambda} (2\hat{a}_{\mathbf{q}_1}^\dagger \hat{a}_{\mathbf{q}_2}^\dagger \hat{a}_{\mathbf{q}_2} \hat{a}_{\mathbf{q}_1} + \hat{a}_{\mathbf{q}_1}^\dagger \hat{a}_{-\mathbf{q}_1}^\dagger \hat{a}_{\mathbf{q}_2} \hat{a}_{-\mathbf{q}_2}) \right. \\ & \left. + \sum_{\mathbf{q} \in \Lambda, \mathbf{q}' \notin \Lambda} (\hat{a}_{\mathbf{q}}^\dagger \hat{a}_{-\mathbf{q}}^\dagger \hat{a}_{\mathbf{q}'} \hat{a}_{-\mathbf{q}'} + \text{H.c.}) \right. \\ & \left. + 4 \sum_{\mathbf{q} \in \Lambda, \mathbf{q}' \notin \Lambda} \hat{a}_{\mathbf{q}}^\dagger \hat{a}_{\mathbf{q}'}^\dagger \hat{a}_{\mathbf{q}} \hat{a}_{\mathbf{q}'} \right). \quad (\text{B2}) \end{aligned}$$

Again one can apply a mean-field (M. F.) approximation and transform  $\hat{V}_{r,r}$  to quadratic form. One may replace  $\langle \hat{a}_{\mathbf{q}}^\dagger \hat{a}_{\mathbf{q}} \rangle = N_r/L_r$  and  $\langle \hat{a}_{\mathbf{q}} \hat{a}_{-\mathbf{q}} \rangle = -iN_r/L_r$  if  $\mathbf{q} \in \Lambda$ . Here  $L_r$  counts the allowed momentum modes in the ring and  $N_r$  is number of particles inside the ring. As discussed earlier for the preheating stage, one thus obtains an effective Hamiltonian containing scattering events between particles on the ring condensate, and all other modes, among ring-condensed modes

and other modes

$$H_{\text{eff}}^r = \sum_{\mathbf{k} \neq \Lambda} (\epsilon_{\mathbf{k}} - J + gn_0 - g\bar{n}_r) \hat{a}_{\mathbf{k}}^\dagger \hat{a}_{\mathbf{k}} + ig\bar{n}_r (\hat{a}_{\mathbf{k}} \hat{a}_{-\mathbf{k}} - \hat{a}_{\mathbf{k}}^\dagger \hat{a}_{-\mathbf{k}}^\dagger), \quad (\text{B3})$$

where  $\bar{n}_r = N_r/V$ . The overall factor of  $i$  before the quadratic interaction term derives from the phase correlation of counterpropagating modes in the ring. This factor may be absorbed via a redefinition of operators,  $\hat{a}_{\mathbf{k}} \rightarrow \exp(-i\pi/4)\hat{a}_{\mathbf{k}}$ . This leads (via a diagonalization) to a set of eigenvalues corresponding to an effective Hamiltonian given by  $\epsilon_{\mathbf{k}}^r = \sqrt{(\epsilon_{\mathbf{k}} - J + gn_0 - g\bar{n}_r)^2 - g^2\bar{n}_r^2}$ . Here we consider the limit  $n_r = n_0$ , where nearly all particles are transferred to the contribution from  $n_r$ .

The key point is that the main consequence of these ring-scattering events is to scatter the particles in the ring back to momenta around  $k \simeq 0$ . This is the counterpart of the cosmological ‘‘back-reaction’’ effect which stabilizes a coexisting BEC (corresponding to simultaneous ring and  $k = 0$  condensates). Ultimately in the ‘‘rescattering’’ phase, collisions between the two lead to a destabilization. In summary, on a timescale  $t \sim t_r$  which corresponds to when the ring BEC has been formed, there will be a counterflow from the ring BEC back to modes at the band minima, until a balance of flow is reached between two BECs.

## 2. Rescattering: Formation of the important cloud state

In this section, we establish a mechanism to destabilize the coexisting BECs, leading to the emergence of a cloud state which represents a proliferation of bosonic pairs.

As in the previous sections, one can write down the scattering terms between the coexisting BECs

$$\hat{V}_{0,r} \equiv \frac{g}{V} \left( \sum_{\mathbf{k} \in \Lambda, \mathbf{q} \neq \Lambda} \hat{a}_{\mathbf{q}}^\dagger \hat{a}_{\mathbf{k}-\mathbf{q}}^\dagger \hat{a}_0 \hat{a}_{\mathbf{k}} + 2 \sum_{\mathbf{k} \in \Lambda} \hat{a}_0^\dagger \hat{a}_{\mathbf{k}}^\dagger \hat{a}_0 \hat{a}_{\mathbf{k}} + 2 \sum_{\mathbf{k} \in \Lambda, \mathbf{q} \neq \Lambda} \hat{a}_0^\dagger \hat{a}_{\mathbf{q}}^\dagger \hat{a}_{\mathbf{q}-\mathbf{k}} \hat{a}_{\mathbf{k}} + 2 \sum_{\mathbf{k} \in \Lambda, \mathbf{q} \neq \Lambda} \hat{a}_{\mathbf{k}}^\dagger \hat{a}_{\mathbf{q}-\mathbf{k}}^\dagger \hat{a}_{\mathbf{q}} \hat{a}_0 \right). \quad (\text{B4})$$

After a mean-field approximation we arrive at an effective Hamiltonian describing scattering events among coexisting BECs and other modes which leads to Eq. (4) in the main text

$$\hat{H}_{\text{eff}}^{0,r} \equiv \sum_{\mathbf{k} \neq \Lambda} (\epsilon_{\mathbf{k}} - J + gn_0/2 - g\bar{n}_r/2 + g\bar{n}_0/2) \hat{a}_{\mathbf{k}}^\dagger \hat{a}_{\mathbf{k}} + 2g\sqrt{\frac{\bar{n}_0\bar{n}_r}{L_r}} \sum_{\mathbf{q} \in \Lambda, \mathbf{k} \neq \Lambda} (\hat{a}_{\mathbf{k}}^\dagger \hat{a}_{\mathbf{q}-\mathbf{k}}^\dagger + \text{H.c.}) + 2g\sqrt{\frac{\bar{n}_0\bar{n}_r}{L_r}} \sum_{\mathbf{q} \in \Lambda, \mathbf{k} \neq \Lambda} (\hat{a}_{\mathbf{k}}^\dagger \hat{a}_{\mathbf{k}-\mathbf{q}}^\dagger + \text{H.c.}). \quad (\text{B5})$$

Here  $\bar{n}_0 = N_0/V$  is the density of  $k = 0$  particles. (Note that the random phase from  $\hat{a}_{\mathbf{q}}$  is unimportant as it can be absorbed into redefined  $\hat{a}_{\mathbf{k}}$  operators.) Importantly, the scattering events here are responsible for states appearing in a new momentum regime. The Hamiltonian is intrinsically nonlocal in momentum space and the exact treatment involves a diagonalization

of a matrix  $M$  which includes multiple degrees of freedom. this leads to an equation of motion for  $a_{\mathbf{k}}$

$$\frac{d}{dt} \hat{a}_{\mathbf{k}}(t) = \frac{-i}{\hbar} \left( \epsilon_{\mathbf{k}}'' \hat{a}_{\mathbf{k}} + \frac{2gn_{\text{geom}}}{\sqrt{L_r}} \sum_{\mathbf{q} \in \Lambda} (\hat{a}_{\mathbf{q}+\mathbf{k}}(t) + \hat{a}_{\mathbf{q}-\mathbf{k}}^\dagger(t)) \right).$$

Here  $\epsilon_{\mathbf{k}}'' = \epsilon_{\mathbf{k}} - J + gn_0/2 - g\bar{n}_r/2 + g\bar{n}_0/2$  and  $n_{\text{geom}} = \sqrt{\bar{n}_0\bar{n}_r}$ . The closed set of equations for all  $k$  modes can be compactly written as

$$\frac{d}{dt} \Psi(t) = \frac{-i}{\hbar} M \Psi(t) \iff \Psi(t) = \exp\{-iMt/\hbar\} \Psi(0),$$

where the vector  $\Psi$  is defined by

$$\Psi(t) = (\hat{a}_{\mathbf{k}_{1,1}}(t) \quad \hat{a}_{-\mathbf{k}_{1,1}}^\dagger(t) \quad \dots \quad \hat{a}_{\mathbf{k}_{L,L}}(t) \quad \hat{a}_{-\mathbf{k}_{L,L}}^\dagger(t))^T. \quad (\text{B6})$$

Here  $\mathbf{k}_{i,j} = \frac{2\pi}{L}(i,j)$ , and  $L$  is the linear size of the system.

Numerically diagonalizing Eq. (B6), we find that the spectrum consists of a large number of of *complex* eigenvalues (see Fig. 6). This can be simply physically interpreted. In particular, since each nonlocal scattering term has a small coefficient, one can deal with each pair of  $(\mathbf{q}, \mathbf{k} - \mathbf{q})$  individually. One may write down the equation of motion for a single pair of momenta [as in Eq. (5) of main text]

$$\frac{d}{dt} \begin{bmatrix} \hat{a}_{\mathbf{k}}(t) \\ \hat{a}_{\mathbf{q}-\mathbf{k}}^\dagger(t) \end{bmatrix} = \frac{-i}{\hbar} \begin{bmatrix} \epsilon_{\mathbf{k}}'' & U' \\ -U' & -\epsilon_{\mathbf{q}-\mathbf{k}}'' \end{bmatrix} \begin{bmatrix} \hat{a}_{\mathbf{k}}(t) \\ \hat{a}_{\mathbf{q}-\mathbf{k}}^\dagger(t) \end{bmatrix}. \quad (\text{B7})$$

Here  $\epsilon_{\mathbf{k}}'' = \epsilon_{\mathbf{k}} - J + gn_0/2 - g\bar{n}_r/2 + g\bar{n}_0/2$  and  $U' \equiv 2g\sqrt{\frac{\bar{n}_0\bar{n}_r}{L_r}}$ . The eigenvalue of the  $2 \times 2$  matrix above is given

by  $\lambda = \frac{\epsilon_{\mathbf{k}}'' - \epsilon_{\mathbf{q}-\mathbf{k}}''}{2} \pm \sqrt{(\frac{\epsilon_{\mathbf{k}}'' + \epsilon_{\mathbf{q}-\mathbf{k}}''}{2})^2 - U'^2}$ . This complex solution reflects exponential growth. Hence, the fastest growing pair is such that  $\epsilon_{\mathbf{k}}'' = -\epsilon_{\mathbf{q}-\mathbf{k}}'' \iff \epsilon_{\mathbf{k}} + \epsilon_{\mathbf{k}-\mathbf{q}} = 2(J - g\bar{n}_0)$ , assuming  $n_0 = \bar{n}_0 + \bar{n}_r$ .

This analysis can be used to determine the shape of the cloud. Consider the following two equations:

$$J \cos(k_y d) + \frac{\hbar^2}{2m} k_x^2 - (J - g\bar{n}_0) = (J - g\bar{n}_0) - J \cos[(k_y - q_y)d] - \frac{\hbar^2}{2m} (k_x - q_x)^2 \\ \text{with } J \cos(q_y d) + \frac{\hbar^2}{2m} q_x^2 = J - gn_0. \quad (\text{B8})$$

The first equation introduces a constraint on the kinetic energy and second equation determines the ring shape. To further simplify these equations, one may cancel  $q_y$  in the first and second equations and find a single equation below

$$0 = J \left( 2 - \frac{\hbar^2 q_x^2}{2mJ} - \frac{gn_0}{J} \right) \cos(k_y d) - 2(J - g\bar{n}_0) \pm J \sin(k_y d) \sqrt{1 - \left( 1 - \frac{\hbar^2 q_x^2}{2mJ} - \frac{gn_0}{J} \right)^2} + \frac{\hbar^2}{2m} (2k_x^2 - 2k_x q_x + q_x^2) \equiv F_{q_x}(\mathbf{k}). \quad (\text{B9})$$

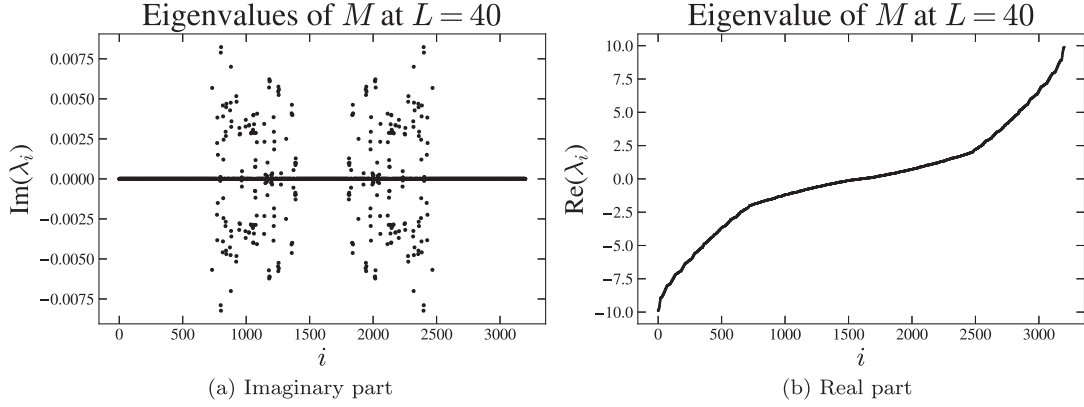


FIG. 6. Eigenvalue of the effective Hamiltonian in Eq. (B5). System size is set to be 40. Panel (a) plots the imaginary part of the eigenvalues. One can observe there are a large number of eigenvalues with a small but finite imaginary part. Panel (b) plots the real part of the eigenvalues. Combining these two figures, one may deduce that there are a large number of complex eigenvalues.

It follows that the cloud shape  $C$  is determined by zeros of the functions  $F_{q_x}(\mathbf{k})$ , where  $q_x$  is a free parameter. Figure 3(b) in the main text is obtained by solving for zeros of these functions numerically.

It is important to stress that after the reheating stage is completed all remnants of “global” coherence decay away at which point the cloud state is fully formed. For the isolated quantum system we study, quantum information cannot be lost, but it can become spread and scrambled in a more complicated manner. Note that the cloud state is a nonthermal state. Nevertheless, we discuss next how it enables the system to thermalize.

### APPENDIX C: THERMALIZATION: BOLTZMANN DYNAMICS

During this last stage of equilibration, the cloud state reorganizes and the collection of nonthermal bosons contained in the cloud begin to occupy the band minimum. This process is associated with Boltzmann dynamics, as it involves no “global” phase coherence. Since we consider weak interactions, one may use leading-order perturbative theory to characterize the processes. The dynamical equation of each  $k$  mode is given by

$$\frac{\partial n_{\mathbf{k}}}{\partial t} = \frac{2g^2}{\hbar} \int \frac{d^2\mathbf{k}' d^2\mathbf{q}}{(2\pi)^4} \Gamma(\mathbf{k}, \mathbf{k}'; \mathbf{k}' + \mathbf{q}, \mathbf{k} - \mathbf{q}) \times 2\pi \delta(\epsilon_{\mathbf{k}} + \epsilon_{\mathbf{k}'} - \epsilon_{\mathbf{k}+\mathbf{q}} - \epsilon_{\mathbf{k}'-\mathbf{q}}). \quad (\text{C1})$$

Here the vertex function  $\Gamma$  determines how the particle number is changed for scattering events involving the four momenta:  $\mathbf{k}, \mathbf{k}', \mathbf{k} + \mathbf{q}, \mathbf{k} - \mathbf{q}'$ :

$$\Gamma(\mathbf{k}, \mathbf{k}'; \mathbf{k} + \mathbf{q}, \mathbf{k} - \mathbf{q}') = n_{\mathbf{k}-\mathbf{q}} n_{\mathbf{k}'+\mathbf{q}} (1 + n_{\mathbf{k}}) (1 + n_{\mathbf{k}'}) - (n_{\mathbf{k}-\mathbf{q}} + 1) (n_{\mathbf{k}'+\mathbf{q}} + 1) n_{\mathbf{k}} n_{\mathbf{k}'}. \quad (\text{C2})$$

The scattering event  $\mathbf{k}, \mathbf{k}' \rightarrow \mathbf{k} - \mathbf{q}, \mathbf{k}' + \mathbf{q}$  decreases  $n_{\mathbf{k}}$  by unity while the reverse process similarly increases  $n_{\mathbf{k}}$ . Note that  $\mathbf{k}, \mathbf{k}' \rightarrow \mathbf{k} - \mathbf{q}, \mathbf{k}' + \mathbf{q}$  and  $\mathbf{k} - \mathbf{q}, \mathbf{k}' + \mathbf{q} \rightarrow \mathbf{k}, \mathbf{k}'$  have different scattering amplitudes. Their difference leads to a

cubic power dependence on the particle number. Thus

$$\frac{\partial n_{\mathbf{k}}}{\partial t} = I_{\mathbf{k}}(n). \quad (\text{C3})$$

This equation reflects three conserved quantities: particle number, momentum, and energy.

Additionally, this Boltzmann dynamics reflects the H theorem which is associated with a monotonic increase in the entropy of the Bose gas discussed in Fig. 4 of the main text and given by

$$S_B = \int d^2\mathbf{k} [(n_{\mathbf{k}} + 1) \ln(n_{\mathbf{k}} + 1) - n_{\mathbf{k}} \ln n_{\mathbf{k}}]. \quad (\text{C4})$$

#### 1. Characterization of cloud state

To understand the equilibrating Boltzmann dynamics, it is important to provide a description of the initial state, the cloud state  $|\Psi_{\Omega}\rangle$ . This is the intermediate nonthermal state which appears after the quenching of the condensate but before thermal equilibrium. It satisfies the following conditions.

(1) It is contained in a simply connected space  $\Omega$  with well defined boundaries in momentum space.  $\Omega$  is, thus, a subspace of the two-dimensional Brillouin zone (BZ). Importantly, the smaller the size of  $\Omega$  the lower the kinetic energy of the system and hence the lower its effective temperature.

(2) For those momentum states which are present there is an effectively large occupation number  $n_{\mathbf{k}}(\Omega) = \langle \Psi_{\Omega} | \hat{n}_{\mathbf{k}} | \Psi_{\Omega} \rangle$ . Indeed in our numerical simulations we find  $n_{\mathbf{k}}(\Omega) \gg 1$ .

(3) Within these occupied states there is no “global” phase coherence

$$\langle \Psi_C | \hat{a}_{\mathbf{k}} \hat{a}_{-\mathbf{k}} | \Psi_C \rangle \ll 1. \quad (\text{C5})$$

The absence of phase coherence means that the cloud state can be treated within a Boltzmann equation approximation.

#### 2. Early stage of Boltzmann dynamics

The dynamics in this early stage strongly depends on these properties of the cloud state. One may classify the two-body collision events according to how many particles inside and outside the cloud are involved. If there are three or four inside-the-cloud modes involved this will induce strong



particle number flow, whereas if there are only two such modes the flow is weaker, and with only one or zero such modes, this contribution in the early dynamics can be ignored.

We focus, for simplicity, on a situation where the particle number distribution in the cloud is uniform. We tested the appropriateness of this assumption numerically and with this assumption, we can greatly simplify the expression for the collision integral. To this end, we define four functions below:

$$\begin{aligned}
F_1(\mathbf{k}) &= \int_{\mathbf{k}_2 \notin C} \frac{d^2 \mathbf{k}_2}{(2\pi)^2} \int_{\mathbf{k}_3 \in C} \frac{d^2 \mathbf{k}_3}{(2\pi)^2} \int_{\mathbf{k}_4 \in C} \frac{d^2 \mathbf{k}_4}{(2\pi)^2} \\
&2\pi \delta(\epsilon_{\mathbf{k}} + \epsilon_{\mathbf{k}_2} - \epsilon_{\mathbf{k}_3} - \epsilon_{\mathbf{k}_4}) (2\pi)^2 \delta(\mathbf{k} + \mathbf{k}_2 - \mathbf{k}_3 - \mathbf{k}_4), \\
F_2(\mathbf{k}) &= \int_{\mathbf{k}_2 \in C} \frac{d^2 \mathbf{k}_2}{(2\pi)^2} \int_{\mathbf{k}_3 \notin C} \frac{d^2 \mathbf{k}_3}{(2\pi)^2} \int_{\mathbf{k}_4 \in C} \frac{d^2 \mathbf{k}_4}{(2\pi)^2} \\
&2\pi \delta(\epsilon_{\mathbf{k}} + \epsilon_{\mathbf{k}_2} - \epsilon_{\mathbf{k}_3} - \epsilon_{\mathbf{k}_4}) (2\pi)^2 \delta(\mathbf{k} + \mathbf{k}_2 - \mathbf{k}_3 - \mathbf{k}_4), \\
G(\mathbf{k}) &= \int_{\mathbf{k}_2 \in C} \frac{d^2 \mathbf{k}_2}{(2\pi)^2} \int_{\mathbf{k}_3 \notin C} \frac{d^2 \mathbf{k}_3}{(2\pi)^2} \int_{\mathbf{k}_4 \notin C} \frac{d^2 \mathbf{k}_4}{(2\pi)^2} \\
&2\pi \delta(\epsilon_{\mathbf{k}} + \epsilon_{\mathbf{k}_2} - \epsilon_{\mathbf{k}_3} - \epsilon_{\mathbf{k}_4}) (2\pi)^2 \delta(\mathbf{k} + \mathbf{k}_2 - \mathbf{k}_3 - \mathbf{k}_4). \\
J(\mathbf{k}) &= \int_{\mathbf{k}_2 \in C} \frac{d^2 \mathbf{k}_2}{(2\pi)^2} \int_{\mathbf{k}_3 \in C} \frac{d^2 \mathbf{k}_3}{(2\pi)^2} \int_{\mathbf{k}_4 \in C} \frac{d^2 \mathbf{k}_4}{(2\pi)^2} \\
&2\pi \delta(\epsilon_{\mathbf{k}} + \epsilon_{\mathbf{k}_2} - \epsilon_{\mathbf{k}_3} - \epsilon_{\mathbf{k}_4}) (2\pi)^2 \delta(\mathbf{k} + \mathbf{k}_2 - \mathbf{k}_3 - \mathbf{k}_4).
\end{aligned}$$

We consider the two separate cases for  $\mathbf{k} \in \Omega$  and  $\mathbf{k} \notin \Omega$ . For the first the collision integral can be reduced to be

$$I_{\mathbf{k}}(n) \simeq \frac{2g^2}{\hbar} [F_1(\mathbf{k})n_{\Omega}^3 - 2F_2(\mathbf{k})n_{\Omega}^3 - G(\mathbf{k})n_{\Omega}^2], \quad (\text{C6})$$

where only the first two terms dominate. Moreover, for  $\mathbf{k} \notin \Omega$  the collision integral becomes

$$I_{\mathbf{k}}(n) \simeq \frac{2g^2}{\hbar} [J(\mathbf{k})n_{\Omega}^3 + F_1(\mathbf{k})n_{\Omega}^2]. \quad (\text{C7})$$

Here numerically one can show that both  $J(\mathbf{k})$  and  $F_1(\mathbf{k})$  nearly vanish except in a small region near the boundary of the cloud.

#### APPENDIX D: RESULTS BASED ON THE GROSS-PITAEVSKII EQUATION

To connect more directly to our numerical GP simulations it is useful to consider the semi-classical approximation of the quantum theory in Eq. (A1) based on the GP equation

$$\left[ J \cos(i\partial_y d) - \frac{\hbar^2 \partial_x^2}{2m} + g|\psi(\mathbf{r}, t)|^2 \right] \psi(\mathbf{r}, t) = i\hbar \frac{\partial}{\partial t} \psi(\mathbf{r}, t).$$

The evolutionary dynamics found in our numerical GP simulations is seen to be consistent with the analytics presented in the previous sections. Also consistent is the close tie to observations from cosmological models. We can demonstrate this through a linearization of the GP equation appropriate to the preheating stage.

In this early stage dynamics (associated with the preheating phase in cosmological models), the physics is governed by a parametric resonance. The initial quenched condensate with a finite kinetic energy can be modeled by the uniform and intrinsically oscillating scalar field  $\psi_0(\mathbf{r}, t) = \sqrt{n_0} e^{-i\omega t}$ .

Here  $\omega$  is the intrinsic oscillating frequency and its value is determined by solving the corresponding GP equation, as we show below. We assume a wave function of the form  $\psi(\mathbf{r}, t) = \psi_0(\mathbf{r}, t) + \delta\psi(\mathbf{r}, t)$ . To linearize the theory, we treat the self-interaction term perturbatively,

$$|\psi(\mathbf{r}, t)|^2 \simeq n_0 + \sqrt{\frac{N}{V}} e^{-i\omega t} \delta\psi^* + \text{H.c.} + O(|\delta\psi|^2). \quad (\text{D1})$$

Now we write down the equation for  $\delta\psi$ . Using the expansion variable  $\delta\psi$ , it follows that

$$\begin{aligned}
&\left[ J \cos(i\partial_y d) - \frac{\hbar^2 \partial_x^2}{2m} + g n_0 + g \sqrt{\frac{N}{V}} e^{-i\omega t} \delta\psi^* \right. \\
&\quad \left. + g \sqrt{\frac{N}{V}} e^{i\omega t} \delta\psi \right] \left( \sqrt{\frac{N}{V}} e^{-i\omega t} + \delta\psi \right) \\
&= i\hbar \partial_t \delta\psi + \hbar \omega \sqrt{\frac{N}{V}} e^{-i\omega t}.
\end{aligned}$$

Since  $\psi_0$  satisfies the GP equation, it follows that

$$\hbar \omega = J + g n_0,$$

indicating that  $\omega$  is intrinsically determined by the model parameters. Keeping only the linear terms in  $\delta\psi, \delta\psi^*$ , one finds

$$\left[ J \cos(i\partial_y d) - \frac{\hbar^2 \partial_x^2}{2m} + 2g n_0 \right] \delta\psi + g n_0 e^{-2i\omega t} \delta\psi^* = i\hbar \partial_t \delta\psi. \quad (\text{D2})$$

One may write the equation in the simple form

$$E_K(-i\nabla) \delta\psi + g(t) \delta\psi^* = i\hbar \partial_t \delta\psi. \quad (\text{D3})$$

where  $E_K(-i\nabla) = J \cos(i\partial_y d) - \frac{\hbar^2 \partial_x^2}{2m} + 2g n_0$  is the single-particle energy with the Hartree-Fock shift and  $g(t) = g n_0 \exp(-2i\omega t)$  is the effective time-dependent interaction. The time dependence originates from the fact that the condensate is intrinsically oscillating. Later we will see how the oscillating  $g(t)$  leads to the parametric instability. Note that in Ref. [11] the modulation of the coupling (to be time dependent) is imposed externally and the oscillating frequency serves as a free parameter of their model. As a contrast, the frequency  $\omega$  is *intrinsic* in our model and has a clear physical origin, the oscillating frequency of the condensate.

Expanding  $\delta\psi = \delta\psi(\mathbf{r}, t) = \sum_{\mathbf{k}, \nu} e^{i\mathbf{k}\cdot\mathbf{r} - i\nu t} \psi_{\mathbf{k}}(\nu)$  and denote  $l_{\mathbf{k}} = J \cos(k_y d) + \frac{\hbar^2 k_x^2}{2m} + 2g n_0$ , Eq. (D2) then becomes

$$l_{\mathbf{k}} \psi_{\mathbf{k}}(\nu) + g n_0 \psi_{-\mathbf{k}}^*(-\nu + 2\omega) = \hbar \nu \psi_{\mathbf{k}}(\nu). \quad (\text{D4})$$

With a change of variable  $\nu = \nu' + \omega$  we arrive at a matrix equation of the form

$$\{ [l_{\mathbf{k}} - \omega] \hat{\sigma}_z + g n_0 \hat{\sigma}_z \hat{\sigma}_x - \nu' \} \begin{bmatrix} \psi_{\mathbf{k}}(\nu' + \omega) \\ \psi_{-\mathbf{k}}^*(\omega - \nu') \end{bmatrix} = 0.$$

Here  $\hat{\sigma}_{x,y,z}$  is the Pauli matrix. Solving this equation, one finds

$$\nu'(\mathbf{k}) = \pm \sqrt{[l_{\mathbf{k}} - \omega]^2 - (g n_0)^2}. \quad (\text{D5})$$

When  $\nu'$  assumes imaginary values, this corresponds to the parametric resonance condition in cosmological models.

When  $\omega$  is taken to be  $(J + gn_0)/\hbar$ , this is consistent with Eq. (A6).

In this way, we show the existence of a parametric instability in an isolated quantum system when the condensate has a finite intrinsic oscillating frequency. The physical process behind the parametric resonance is that the energy of the condensate transfers to the noncondensate particles in an exponentially amplified way.

### GP derivation of the cloud thermalization stage:

#### Comparison with the quantum Boltzmann equation

It is instructive to use the machinery of the GP equation to characterize how equilibration occurs. We will begin with a stage in which there is no “global” phase coherence and write  $\psi(\mathbf{r}, t) = \sum_{\mathbf{k}} \psi_{\mathbf{k}}(t)e^{i\mathbf{k}\mathbf{r}}$ , the corresponding equation of motion in terms of the complex scalar field  $\psi_{\mathbf{k}}(t)$  is then

$$i\hbar \frac{\partial \psi_{\mathbf{k}}(t)}{\partial t} = \epsilon_{\mathbf{k}} + g \sum_{\mathbf{k}_1, \mathbf{k}_3} \psi_{\mathbf{k}_1}^* \psi_{\mathbf{k}_3} \psi_{\mathbf{k}_4}, \quad (\text{D6})$$

where  $\mathbf{k}_4 = \mathbf{k} + \mathbf{k}_1 - \mathbf{k}_3$ . For simplicity, we put  $\psi_{\mathbf{k}}(t) = \tilde{\psi}_{\mathbf{k}}(t)e^{-i\epsilon_{\mathbf{k}}t/\hbar}$ . We then arrive at

$$i\hbar \frac{\partial \tilde{\psi}_{\mathbf{k}}(t)}{\partial t} = g \sum e^{i(\epsilon_i - \epsilon_f)t/\hbar} \tilde{\psi}_{\mathbf{k}_1}^* \tilde{\psi}_{\mathbf{k}_3} \tilde{\psi}_{\mathbf{k}_4}, \quad (\text{D7})$$

where  $\epsilon_i = \epsilon_{\mathbf{k}_3} + \epsilon_{\mathbf{k}_4}$ ,  $\epsilon_f = \epsilon_{\mathbf{k}} + \epsilon_{\mathbf{k}_1}$ ,  $n_{\mathbf{k}} = \psi_{\mathbf{k}}^* \psi_{\mathbf{k}} = \tilde{\psi}_{\mathbf{k}}^* \tilde{\psi}_{\mathbf{k}}$ . We now assume that, in addition to the absence of “global” phase coherence, the interaction energy is quite small. As a result, the time change of  $\tilde{\psi}_{\mathbf{k}}(t)$  can be approximated to the first order in  $g$  and the change rate is much smaller than  $\epsilon_i/\hbar$ ,  $\epsilon_f/\hbar$ . We then obtain

$$\tilde{\psi}_{\mathbf{k}}(t) \approx \tilde{\psi}_{\mathbf{k}}(0) - i\pi g \sum \delta(\epsilon_i - \epsilon_f) \tilde{\psi}_{\mathbf{k}_1}^* \tilde{\psi}_{\mathbf{k}_3} \tilde{\psi}_{\mathbf{k}_4}. \quad (\text{D8})$$

Now because of the lack of phase coherence, different  $\tilde{\psi}$  amplitudes have uncorrelated random phases. Only terms with both  $\psi$  and  $\psi^*$  of the same momentum will survive in the

equation. Therefore, combining Eqs. (D7) and (D8), we find

$$\frac{\partial n_{\mathbf{k}}}{\partial t} = \frac{4\pi g^2}{\hbar} \sum_{\mathbf{k}_1, \mathbf{k}_3} \delta(\epsilon_i - \epsilon_f) (n_{\mathbf{k}_1} n_{\mathbf{k}_3} n_{\mathbf{k}_4} + n_{\mathbf{k}} n_{\mathbf{k}_3} n_{\mathbf{k}_4} - n_{\mathbf{k}} n_{\mathbf{k}_1} n_{\mathbf{k}_3} - n_{\mathbf{k}} n_{\mathbf{k}_1} n_{\mathbf{k}_4}). \quad (\text{D9})$$

Comparing this result with Eq. (C2), we find that the term  $n_{\mathbf{k}_3} n_{\mathbf{k}_4} - n_{\mathbf{k}} n_{\mathbf{k}_1}$  is missing in this approximate GP approach. Thus, the GP approach works best in the early stages of thermalization where the leading contribution is  $\propto n^3$ . We chose a large particle density for our simulations to ensure this dominance of  $n^3$  in the early stage. We infer that there may be some discrepancies at very late times.

### APPENDIX E: NUMERICAL PARAMETERS IN THE GROSS-PITAEVSKII SIMULATIONS

The parameters we used for the simulations are:  $V_1 = 12E_R$ ,  $V_2 = 2E_R$ ,  $gn_0 = 0.015E_R$ ,  $h/T = 4.75E_R$ , where  $E_R = \hbar^2(\pi/d)^2/2m$  is the recoil energy unit.  $d$  is the period of the lattice, which is discretized into 64 grids in the  $y$  direction with a total length of  $256d$ . For the  $x$  direction which is free and thus insensitive to grid resolution, we use  $64d$  for the total length to speed up the simulations. Periodic boundary conditions are imposed for all directions. We run the dynamics of the system for a sufficiently long time until we find the results are stable. The longest running time is 6000 T.

In our simulations, noise is added only at the earliest time ( $t = 0$ ) in the sequence and dropped thereafter. This plays the physical role of random quantum fluctuations. Once the dynamics is initiated in this way no noise or other external perturbations are present. We emphasize the dynamical evolution we consider is for a closed system.

Our simulations involve graphics processing unit based quasispectral, split-step method to solve the GP equation based on fast Fourier transforms. More details can be found in Ref. [36].

- 
- [1] J. L. Miller, The early universe in a quantum gas, *Phys. Today* **76**(1), 14 (2023).
- [2] C. L. Hung, V. Gurarie, and C. Chin, From cosmology to cold atoms: Observation of Sakharov Oscillations in a quenched atomic superfluid, *Science* **341**, 1213 (2013).
- [3] S. Eckel, A. Kumar, T. Jacobson, I. B. Spielman, and G. K. Campbell, A rapidly expanding Bose-Einstein Condensate: An expanding universe in the lab, *Phys. Rev. X* **8**, 021021 (2018).
- [4] C. Neuenhahn and F. Marquardt, Quantum simulation of expanding space-time with tunnel-coupled condensates, *New J. Phys.* **17**, 125007 (2015).
- [5] J. Berges, A. Rothkopf, and J. Schmidt, Nonthermal fixed points: Effective weak coupling for strongly correlated systems far from equilibrium, *Phys. Rev. Lett.* **101**, 041603 (2008).
- [6] V. Kasper, F. Hebenstreit, M. K. Oberthaler, and J. Berges, Schwinger pair production with ultracold atoms, *Phys. Lett. B* **760**, 742 (2016).
- [7] J. Berges, K. Boguslavski, S. Schlichting, and R. Venugopalan, Universality far from Equilibrium: From Superfluid Bose gases to heavy-ion collisions, *Phys. Rev. Lett.* **114**, 061601 (2015).
- [8] J. Berges, Controlled nonperturbative dynamics of quantum fields out of equilibrium, *Nucl. Phys. A* **699**, 847 (2002).
- [9] J. Berges and D. Sexty, Bose-Einstein condensation in relativistic field theories far from equilibrium, *Phys. Rev. Lett.* **108**, 161601 (2012).
- [10] J. Eisert, M. Friesdorf, and C. Gogolin, Quantum many-body systems out of equilibrium, *Nat. Phys.* **11**, 124 (2015).
- [11] A. Chatrchyan, K. T. Geier, M. K. Oberthaler, J. Berges, and P. Hauke, Analog cosmological reheating in an ultracold Bose gas, *Phys. Rev. A* **104**, 023302 (2021).
- [12] C. Viermann, M. Sparn, N. Liebster, M. Hans, E. Kath, Á. Parra-López, M. Tolosa-Simeón, N. Sánchez-Kuntz, T. Haas, H. Strobel *et al.*, Quantum field simulator for dynamics in curved spacetime, *Nature (London)* **611**, 260 (2022).
- [13] E. A. Calzetta and B. L. Hu, Early universe quantum processes in bec collapse experiments, *Int. J. Theor. Phys.* **44**, 1691 (2005).
- [14] D. Faccio, F. Belgiorno, S. Cacciatori, V. Gorini, S. Liberati, and U. Moschella, *Analogue Gravity Phenomenology*:

- Analogue sSpacetimes and Horizons, From Theory to Experiment* (Springer, New York, 2013), Vol. 870.
- [15] L. V. Keldysh, Diagram technique for nonequilibrium processes, *Zh. Eksp. Teor. Fiz.* **47**, 1515 (1964).
- [16] J. Schwinger, Brownian motion of a quantum oscillator, *J. Math. Phys.* **2**, 407 (1961).
- [17] O. V. Konstantinov and V. I. Perel, A graphical technique for computation of kinetic quantities, *Zh. Eksp. Teor. Fiz.* **39**, 1960 (1960).
- [18] L. P. Kadanoff and G. Baym, *Quantum Statistical Mechanics* (W.A. Benjamin, New York, 1962).
- [19] M. Srednicki, Chaos and quantum thermalization, *Phys. Rev. E* **50**, 888 (1994).
- [20] A. Pal and D. A. Huse, Many-body localization phase transition, *Phys. Rev. B* **82**, 174411 (2010).
- [21] R. Moessner and S. L. Sondhi, Equilibration and order in quantum Floquet matter, *Nat. Phys.* **13**, 424 (2017).
- [22] P. O. Fedichev and U. R. Fischer, Gibbons-hawking effect in the sonic de sitter space-time of an expanding Bose-Einstein-condensed gas, *Phys. Rev. Lett.* **91**, 240407 (2003).
- [23] U. R. Fischer and R. Schützhold, Quantum simulation of cosmic inflation in two-component Bose-Einstein condensates, *Phys. Rev. A* **70**, 063615 (2004).
- [24] S.-Y. Chä and U. R. Fischer, Probing the scale invariance of the inflationary power spectrum in expanding quasi-two-dimensional dipolar condensates, *Phys. Rev. Lett.* **118**, 130404 (2017).
- [25] L. Senatore, Lectures on inflation, *Theoretical Advanced Study Institute in Elementary Particle Physics: New Frontiers in Fields and Strings*, in *New Frontiers in Fields and Strings* (World Scientific, Singapore, 2016), Chap. 8, pp. 447–543.
- [26] M. Forconi, W. Giarè, E. Di Valentino, and A. Melchiorri, Cosmological constraints on slow roll inflation: An update, *Phys. Rev. D* **104**, 103528 (2021).
- [27] R. Allahverdi, R. Brandenberger, F.-Y. Cyr-Racine, and A. Mazumdar, Reheating in inflationary cosmology: Theory and applications, *Annu. Rev. Nucl. Part. Sci.* **60**, 27 (2010).
- [28] D. Baumann, Tasi lectures on inflation, [arxiv:0907.5424](https://arxiv.org/abs/0907.5424).
- [29] A. Albrecht and P. J. Steinhardt, Cosmology for grand unified theories with radiatively induced symmetry breaking, *Phys. Rev. Lett.* **48**, 1220 (1982).
- [30] L. Kofman, A. Linde, and A. A. Starobinsky, Reheating after inflation, *Phys. Rev. Lett.* **73**, 3195 (1994).
- [31] V. Sharma, S. Choudhury, and E. J. Mueller, Dynamics of Bose-Einstein recondensation in higher bands, *Phys. Rev. A* **101**, 033609 (2020).
- [32] X.-Q. Wang, G.-Q. Luo, J.-Y. Liu, W. V. Liu, A. Hemmerich, and Z.-F. Xu, Evidence for an atomic chiral superfluid with topological excitations, *Nature (London)* **596**, 227 (2021).
- [33] H. Fu, A. Glatz, F. Setiawan, K.-X. Yao, Z. Zhang, C. Chin, and K. Levin, Dynamical preparation of an atomic condensate in a hofstadter band, *Phys. Rev. A* **105**, 043301 (2022).
- [34] This parametric resonance, in contrast to Ref. [11], is naturally associated with the intrinsic dynamics of the isolated system and does not require an externally imposed time-dependent interaction, as discussed in Appendix A.
- [35] C. J. Kennedy, W. C. Burton, W. C. Chung, and W. Ketterle, Observation of Bose–Einstein condensation in a strong synthetic magnetic field, *Nat. Phys.* **11**, 859 (2015).
- [36] D. Pathria and J. L. Morris, Pseudo-spectral solution of nonlinear schrödinger equations, *J. Comput. Phys.* **87**, 108 (1990).
- [37] P. Scherpelz, K. Padavić, A. Raçon, A. Glatz, I. S. Aranson, and K. Levin, Phase imprinting in equilibrating Fermi gases: The transience of vortex rings and other defects, *Phys. Rev. Lett.* **113**, 125301 (2014).
- [38] L. F. Abbott, E. Farhi, and M. B. Wise, Particle production in the new inflationary cosmology, *Phys. Lett. B* **117**, 29 (1982).
- [39] J. H. Traschen and R. H. Brandenberger, Particle production during out-of-equilibrium phase transitions, *Phys. Rev. D* **42**, 2491 (1990).
- [40] G. Felder, J. García-Bellido, P. B. Greene, L. Kofman, A. Linde, and I. Tkachev, Dynamics of symmetry breaking and tachyonic preheating, *Phys. Rev. Lett.* **87**, 011601 (2001).
- [41] L. Feng, L. W. Clark, A. Gaj, and C. Chin, Coherent inflationary dynamics for Bose-Einstein condensates crossing a quantum critical point, *Nat. Phys.* **14**, 269 (2018).
- [42] For a given  $\mathbf{k}$  (denoted by the orange dot), the red dashed curves denote the ring modes ( $\Lambda$ ) shifted by momentum  $-\mathbf{k}$  and the blue dashed curves represent the equienergy lines with energy  $-\epsilon_{\mathbf{k}}$ . Their intersection gives the resonant  $\mathbf{q} = \mathbf{k}$  mode satisfying both momentum and energy conservation conditions.
- [43] D. T. Son, Reheating and thermalization in a simple scalar model, *Phys. Rev. D* **54**, 3745 (1996).
- [44] K. D. Lozanov and M. A. Amin, End of inflation, oscillons, and matter-antimatter asymmetry, *Phys. Rev. D* **90**, 083528 (2014).
- [45] M. A. Amin, R. Easther, H. Finkel, R. Flauger, and M. P. Hertzberg, Oscillons after inflation, *Phys. Rev. Lett.* **108**, 241302 (2012).
- [46] I. Tkachev, S. Khlebnikov, L. Kofman, and A. Linde, Cosmic strings from preheating, *Phys. Lett. B* **440**, 262 (1998).
- [47] Planck 2015 results - xiii. cosmological parameters, *A&A* **594**, A13 (2016).
- [48] V. E. Zakharov, V. S. L'vov, and G. Falkovich, Statistical description of weak wave turbulence, in *Kolmogorov Spectra of Turbulence I: Wave Turbulence* (Springer, Berlin, 1992), pp. 63–82.
- [49] This was not previously reported but it can be seen from Fig. 7 in Ref. [33].
- [50] L. Kofman, A. Linde, and A. A. Starobinsky, Towards the theory of reheating after inflation, *Phys. Rev. D* **56**, 3258 (1997).
- [51] To observe why  $\mathbf{q}_1 = -\mathbf{q}_2$  is the leading contribution, one may define  $f(Q)$  as the multiplicity for the space  $q_1 + q_2 = Q$ , i.e.,  $f(Q) = \text{number of elements in } \{(q_1, q_2) | q_1 + q_2 = Q, q_{1,2} \in \Lambda\}$ . One can check that, for the ring-shaped  $\Lambda$ ,  $f(Q)$  is on the order of 1 if  $Q \neq 0$  while for  $Q = 0$ ,  $f(Q)$  is of the order  $L \gg 1$ .